The Changing Circulation of Asia-Pacific Marginal Seas in the South China Sea: a Physical View

Jianping Gan[1], Zhiqiang Liu[2], Chiwing Rex Hui[1], Yao Tang[1], Zhongya Cai[1] and Junlu Li[1]

[1:] Department of Ocean Science and Department of Mathematics, Hong Kong University of Science and Technology, Kowloon, Hong Kong, China

[2:] Department of Ocean Science and Engineering, Southern University of Science and Technology, Shen Zhen, China

Citation: **Gan, J**., Z. Liu, Rex Hui, Y. Tang, Z. Cai and J. Li, 2020. The Changing Circulation of Asia-Pacific Marginal Seas in the South China Sea: a Physical View *The Changing Asia-Pacific Marginal Seas*, ed. by Arthur Chen and Xinyu Guo. Springer.

Table of Contents

1. Introduction

The South China Sea (SCS) is a semi-enclosed marginal sea in the tropical northwest Pacific Ocean (NPO, Fig. 1). Four restricted openings connect the SCS to surrounding seas. The shallow (<100 m) Taiwan and Karimata Straits connect the northern (NSCS, north of 13°N) and southern SCS (SSCS) to the East China Sea (ECS) and Java Sea, respectively. The channels (<200 m) in the Palawan Archipelago join the southeastern SCS to the Sulu Sea with the strongest water exchange in those channels occurring through Mindoro Strait. Because of the strong exchange through Mindoro Strait, this strait aptly represents the flow through the channels of the Palawan Archipelago. Lastly, Luzon Strait (LS), northeast of the SCS, is the deepest passage (~2500 m) connecting the SCS to the NPO.

The maximum water depth of the deep SCS basin is over 4000 m, and below 2500 m, the basin is enclosed. There are broad continental shelves on the western sides of the NSCS and the SSCS, and the central basin is surrounded by a semi-enclosed continental slope between the 200 m and 3000 m isobaths. The topography of the slope is highly variable containing valleys, canyons, seamounts, and ridges. The SCS has a deep basin in the northeast and a shallower basin south of 9°N in the SSCS (Fig. 1). The 3000 m isobath enclosing the southern basin is shaped like a rhombus with a moderate slope that is oriented northeastward.

The mean annual SCS circulation flows cyclonically in the upper layer (<~750 m) along the sea's surrounding slope (Gan et al. 2016b). This circulation pattern comes from the intrusion of the Kuroshio Current through LS in the upper layer and from positive vorticity caused by the monsoonal wind stress curl. The circulation weakens along the southwestward mainstream over the slope in the NSCS. The mainstream bifurcates near the Xisha Islands and forms an even weaker southeastward branch that flows towards Mindoro Strait. The main branch flows further southward along the slope and intensifies over the narrow slope east of Vietnam. Part of this relatively weak western boundary current in the SCS basin veers northeastward in the southernmost SSCS, joins the southeastward branch from the Xisha Islands, and exits the SCS through Mindoro Strait (Liu and Gan 2017). The southward transport across the SCS basin is called the SCS Throughflow (SCSTF) (Qu et al. 2006), and it conveys the NPO waters through LS to the Java Sea, ECS, and the Sulu Sea (Qu, 2000; Qu et al. 2000). In addition, the circulation in the upper layer of the SCS

has strong seasonal variation that is subject to the controlling variability of the Kuroshio intrusion through LS and of the monsoonal wind stress (Gan et al. 2006).

The monsoonal wind and the water intrusions/extrusions through the surrounding straits, jointly drive the SCSTF, especially through LS (Gan et al. 2006; Gan et al. 2016a). Through LS, there is a three-layered exchange flow that connects with the three-layered circulation in the SCS basin (Gan et al. 2016a; Gan et al. 2016b; and Xu and Oey 2014). In the upper layer of LS, the Kuroshio carries the NPO water and branches westward (Wu and Hsin 2012) connecting to the other surrounding seas via the SCSTF (Fang et al. 2009). In the intermediate layer of LS, there is an eastward outflow of SCS water (Gan et al. 2016b; Li and Qu 2006). Finally, in the lower layer of LS (1500 to 2500 m), the intrusion of denser NPO water regulates the thermal dynamics in the deep basin (Nan et al. 2015). The intrusive denser NPO water sinks in the NSCS and causes an energetic cyclonic circulation in the closed deep basin (Lan et al. 2013). There is extensive upwelling over the slope in the northwestern SCS and east of Vietnam to compensate for these subducted waters (Chao et al. 1996), and the SCSTF is partly maintained by the upwelled denser waters (Qu et al. 2009).

In this chapter, we use recent observations and model results from the China-Seas Multi-scale Ocean Modeling System (CMOMS, https://odmp.ust.hk/cmoms/) (Gan et al. 2016b) to present characteristics of the circulation in the SCS. We describe new knowledge of the mean states, multiscale variabilities, and forcing mechanisms. Section 2 introduces the mean state of internal and external forces that drive the SCS circulation. Section 3 discusses the general nature of SCS circulation and the hydrographic properties. Section 3 also highlights the circulation pathways in the SCS basin indicated by residence time of different water masses. Section 4 presents the variability of the forcing and the changing SCS circulation. We discuss the mechanism that governs the SCS circulation and its variability in Section 5, and, finally, in Section 6, we summarize the contents of the chapter.

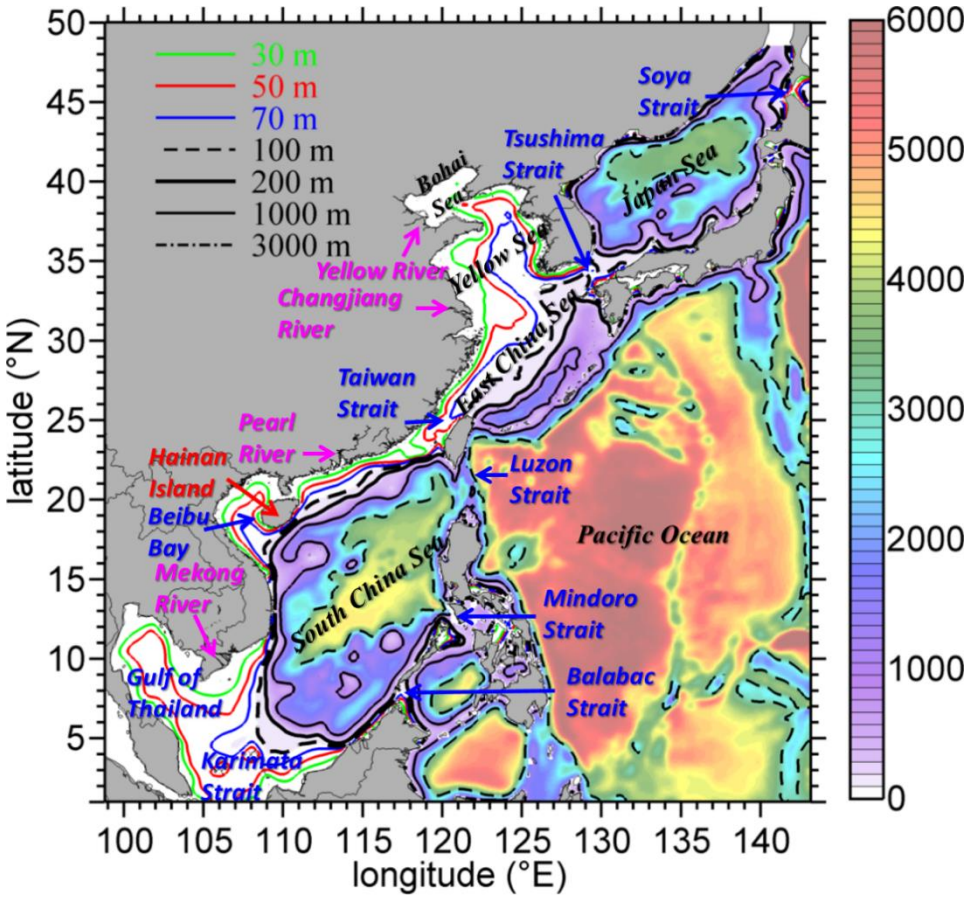

Fig. 1. Bathymetry (m) in the Northwest Pacific Ocean and China Seas with the 30, 50, 70, 100, 200, 1000, and 3000 m isobaths contours. The locations of seas, islands, rivers, and straits are marked (adapted from Gan et al. 2016b).

2. Characteristics of internal and external forces in the SCS

First, we introduce the characteristics of forces that drive the circulation in the SCS. We focus on the major external drivers: wind forcing and volume transport through the straits around the basin.

2.1 The monsoonal wind

The East Asia Monsoon is the primary influence on the upper layer circulation. In winter, the northeasterly wind prevails over the entire SCS basin with an average wind speed of ~9 m s^{-1} (Hellerman and Rosenstein 1983). In summer, the southwesterly wind has an average speed of ~6 m s^{-1}. The winter monsoon is much stronger than the southwesterly summer wind. The line of zero wind stress curl orients northeast to southwest over the central basin and forms a dipole wind stress curl pattern with negative/positive values in the northern/southern part of basin. In winter, the

positive wind stress curl is stronger than in summer; for example, over the slope east of Vietnam. In summer, a dipole wind stress curl also exists, but with positive/negative values in the northern/southern part of basin, opposite to the winter dipole.

2.2 External transport through straits

The exchange flows around the periphery of the SCS vary coherently with the current in the NPO. In the tropical NPO, the westward North Equatorial Current (NEC) between 8°N and 18°N bifurcates at ~11°N east of the Philippines in summer and at ~14°N in winter. The bifurcation is shown by the transport stream function in the upper 750 m in Fig. 2. The annual mean transport of the NEC is ~59 Sv. The bifurcation of the NEC forms the northward Kuroshio (~23 Sv) and the southward Mindanao Current (~35 Sv) (Fig. 2). Because of the weakened NEC transport and the northward displacement of its stream-axis, in winter there is a weaker Kuroshio transport with a stronger westward intrusion into the SCS through LS (Qu, 2000; Qu et al. 2000) and across the slope of the ECS (Liu and Gan 2012).

Fig. 3 illustrates the exchange between the SCS and adjacent seas and the transport coherencies. An ~5.5 Sv (annual and depth-integrated transport) westward transport enters the SCS basin through LS from the NPO. Conveyed by the slope in the SCS, an ~1.2 Sv of this intrusive transport exits the basin through Taiwan Strait in the north, an ~1.16 Sv exits through Karimata Strait, and an ~3.2 Sv transport exits through the Mindoro Strait in the south. These transports around the periphery of the SCS are closely connected with the transports in neighboring seas because of mass conversation and constraining shelf topography of the East Asia marginal sea. For example, an ~1.2 Sv northward transport in Taiwan Strait is closely linked with the shoreward transport across the slope off the ECS and the northward transport through Tsushima Strait. These linked transports interact with the wind-forced currents and shape the circulation in the SCS (Gan et al. 2016b).

The different flow exchanges have strong seasonality around the periphery of the SCS. In addition, the transports in the four straits concurrently exhibit a strong annual *U*-shaped (or inverted *U*-shaped) time variation, with weaker inflows/outflows in summer and stronger ones during the other seasons (Fig. 3). We extrinsically link the *U*-shaped variation of the transports with the variable strength of the Kuroshio separation at the entrance of LS (Hsin et al. 2012; Qu et

al. 2000; Wu and Hsin 2012) and intrinsically link the same variation with the interaction between the transports and the SCS circulation (Gan et al. 2016a; Gan et al. 2016b).

Not only do the transports that cross through the straits and slope vary geographically and seasonally, but these transports also vary vertically. The transports in the deeper layer are much weaker than the ones in the upper layer. In LS, the inflow-outflow-inflow structure is evident in the upper-middle-deep layers. Although the complete mechanism governing the three-layer structure is still unclear, it is conceivable that this sandwich structure is responsible for the alternating three-layer cyclonically-anticyclonically-cyclonically (CAC) spinning circulation in the SCS (Gan et al. 2016a). We estimate that the transports in the upper, middle, and deep layers of LS are ~-5.9 Sv, 1.4 Sv, and -0.9 Sv, respectively. An ~3.2 Sv outward transport in the Mindoro Strait occurs in the upper 400 m while there is a weak inflow of ~0.1 Sv in the deep channels of the main Mindoro Strait channel. The inflow from LS in the upper layer of the SCS basin balances the outflows through Taiwan Strait, Karimata Strait, and Mindoro Strait. Liu and Gan (2017) found that a downward momentum flux from the upper layer of LS and an upward momentum flux from the deep layer compensate for the outflow in the middle layer of LS. On the domain-averaged scale, little of the deep intrusive water reaches the upper layer, but a strong upward motion can occur in isolated locations in the SCS because of local topography, eddies, waves, and other local processes. By generating the upward motion in the semi-closed basin, deep transport, such as the one in LS, is important in maintaining the three-dimensional SCS circulation.

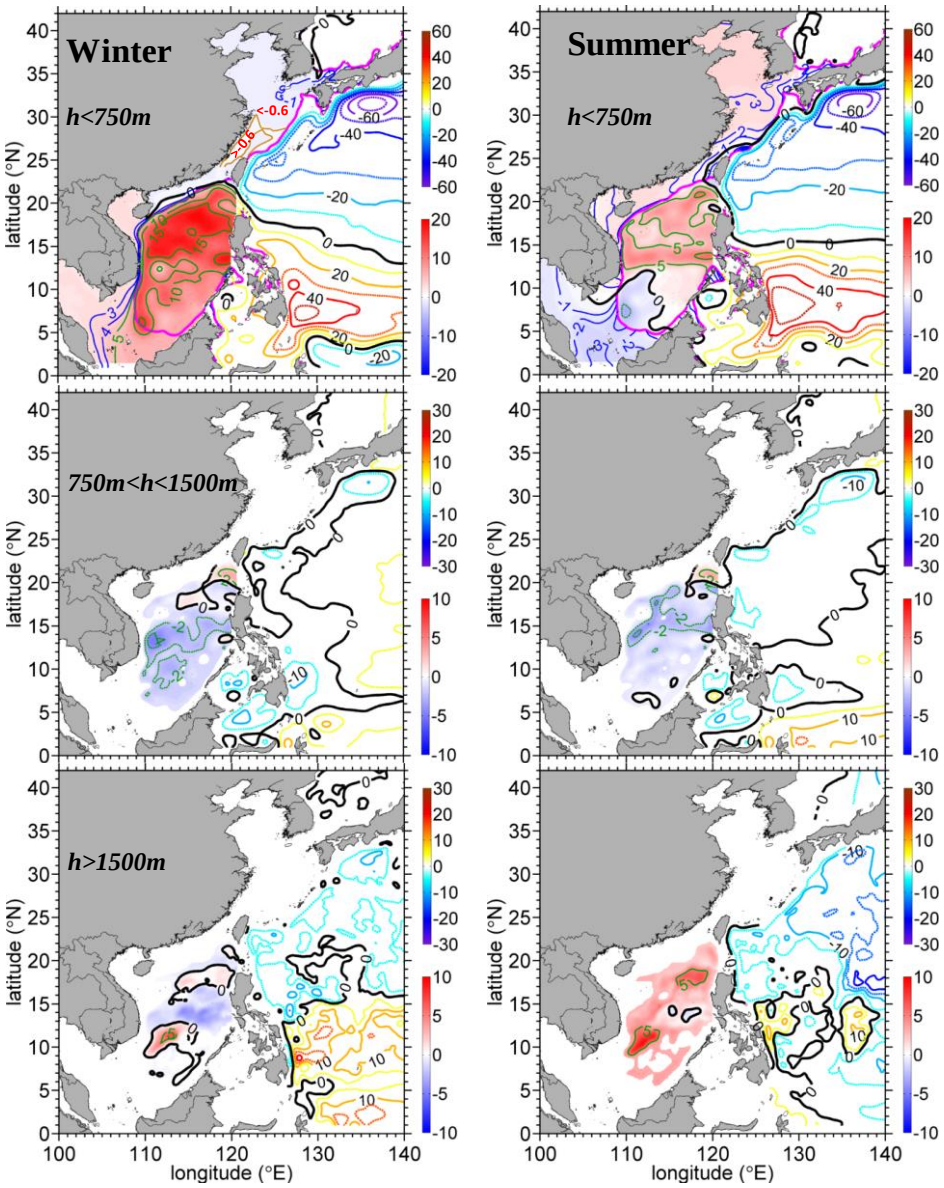

Fig. 2. Transport (Sv) stream functions in the upper layer (<750 m), middle layer (750 to 1500 m), and deep layer (>1500 m) in the winter (left column) and summer (right column), respectively. The upper and lower scales are for the western Pacific (east of the 200 m isobath) and the SCS, respectively (adapted from Gan et al. 2016b).

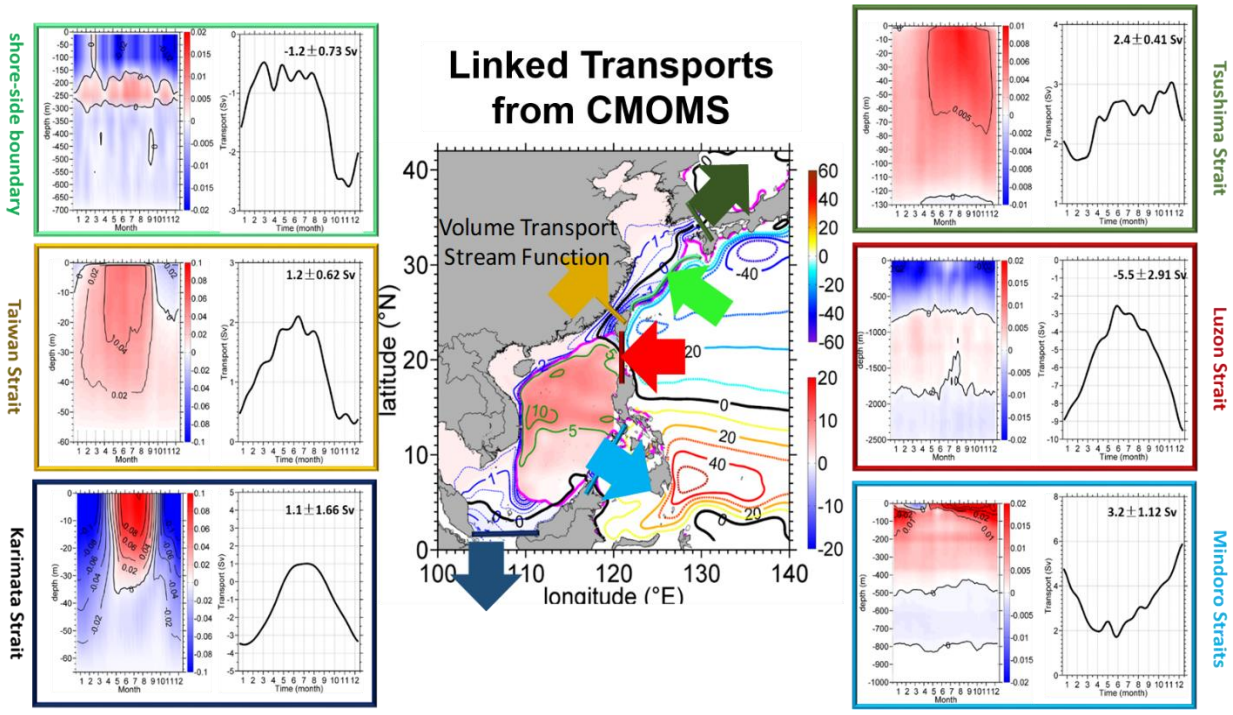

Fig. 3. Time series of depth-integrated transport (Sv) and depth-dependent volume flux (m^2 s^{-1}) through the straits around the South China Sea. Each strait and shore-side-boundary of Kuroshio along the ECS slope is represented by a specific color bar and the result for each strait is shown by a corresponding colored box. The background contours in the surrounding China Seas represent the annual mean transport stream function for the upper 750 m. A positive value refers to northward flow in the Taiwan, Karimata, and Tsushima Straits, and outflows in Luzon and Mindoro Straits. The pink line represents the 200 m isobath (redrawn from Gan et al. 2016b).

3. Circulation and physical characteristics in the SCS

In this section, we introduce the general oceanic response of the SCS to forcing conditions.

3.1 SCS layered circulation

The time-dependent, three-dimensional circulation of the China Seas in winter and summer are represented in Fig. 2 by the depth-integrated stream function (ψ) for the upper, middle, and deep layers. The time series of depth-dependent horizontally averaged vorticity in the SCS is shown in Fig. 4. The circulation in the SCS is characterized by a three-layer alternating spinning CAC circulation in the upper (<750 m), middle (750-1500 m), and deep layers (>1500 m). The CAC circulation is closely linked with the external transports through the surrounding straits and

the monsoonal wind (Gan et al. 2016a). We present an overview of flow in the three layers in the following paragraphs.

Upper layer (0-750 m): In the NPO, the NEC and the Kuroshio are major currents adjacent to the SCS. The two currents exhibit strong seasonality, as indicated by ψ in Fig. 2, and the currents strongly influence the upper layer flow in the SCS because of the NEC's bifurcation.

In winter, a weakened NEC bifurcates further north than in summer. This bifurcation, in turn, weakens the Kuroshio and enhances the westward intrusion of the Kuroshio into the SCS through LS (Gan et al. 2006; Qu, 2000; Qu et al. 2000). As a result, the SCS winter circulation in the upper layer flows cyclonically and spans the entire basin more strongly in the northern part of the SCS basin than in the south (Fig. 2). In addition to the stronger winter Kuroshio intrusion, this upper layer circulation is forced by the northeasterly monsoon and its associated positive wind stress curl (Gan et al. 2006; Qu, 2000).

In summer, a southwestward current along the northern slope and an eastward returning current at ~13°N form a cyclonic circulation in the northern part of the basin and a weak anticyclonic circulation in the southern part of the basin. Together, the basin dipole wind stress curl and the recirculation of a coastal jet separation east of Vietnam (Gan and Qu 2008) govern the summer circulation.

The half-basin circulation patterns in both seasons produce a larger outflow through Mindoro Strait than through Karimata Strait and Taiwan Strait. This larger outflow indicates that the LS inflow exits the SCS mainly through Mindoro Strait which is the main pathway of the SCSTF (Qu et al. 2006).

Middle layer (750-1500 m): In the middle layer, the current in the NPO is generally weak in winter and summer. The circulation in the middle layer of the SCS itself flows anticyclonically, though it is not as circular as in the upper layer. The seasonality of the mid-layer circulation is also much weaker than in the upper layer. The main external forcing for the anticyclonic circulation is the outflow in LS, while the internal forcing is complex and involves the interaction among the layers and the effect of slope topography. More details about the forcing mechanism are presented in Section 5.

Deep layer (>1500 m): In the deep layer, a cyclonic circulation prevails in the basin in winter and summer (Lan et al. 2013). There is cyclonic basin circulation in this layer, despite a weak anticyclonic circulation in the deepest central basin in winter. The cyclonic circulation is stronger in summer than in winter, which is different from the upper layer where the cyclonic circulation is stronger in winter. The seasonality correlated well in time with the deep intrusion through LS.

All three layers have seasonal variability. We examine the seasonal variation of the layered circulation more closely using the time series of domain-averaged vorticity obtained from the numerical solution to Stokes' theorem:

$$C = \oint \vec{V} \cdot dl = \oiint \zeta dS, \quad (1)$$

where $\vec{V}$ is the velocity vector and ζ is the vertical relative vorticity normal to *S*, which is the area of the sea having the layered circulation, *C*. We exclude the shelf where the depth is less than 100 m in the SCS to rule out the influence of shelf circulation (Gan et al. 2009a; Gan et al. 2009b). The numerical model results for Equation (1) are displayed in Fig. 4 showing the vertical circulation patterns of the SCS.

The layered circulation in the SCS is physically valid only under the principles governing Stokes' Theorem (Equation 1) with a geopotential coordinate system. The 'layered circulation' observed in other studies is detected by an overhead view of the circulation pattern over only part of the basin which was never physically sufficient. Meanwhile, the circulation exposed by Equation (1) in an isopycnal coordinate system might not be valid for proving the existence of CAC circulation because the area-integrated vorticity perpendicular to the isopycnal surface cannot adequately represent the layered circulation in the SCS. Details about the physical definition of the layered circulation in a basin are presented in Cai et al. (2019).

As we previously stated, the time series of domain-averaged vorticity in Fig. 4 presents a three-layer alternating CAC rotating circulation in the SCS. Furthermore, Fig. 4 and Fig. 2 illustrate the seasonality of the circulation. In the upper layer, vorticity input from the wind stress curl and a positive horizontal shear vorticity on the seaward side of the slope current jointly form the cyclonic circulation. In winter, the slope current and the basin circulation is much stronger (Fig. 2). The stronger slope current and basin circulation result in a thicker (thinner) upper layer during

winter (summer) because of the first order conservation of potential vorticity. However, in the middle layer, the basin circulation is anticyclonic for the entire year, and it is relatively strong in late spring and early summer. In the deep layer, the cyclonic circulation strengthens from July to October, and a relatively strong circulation occurs between 2000 and 3000 m.

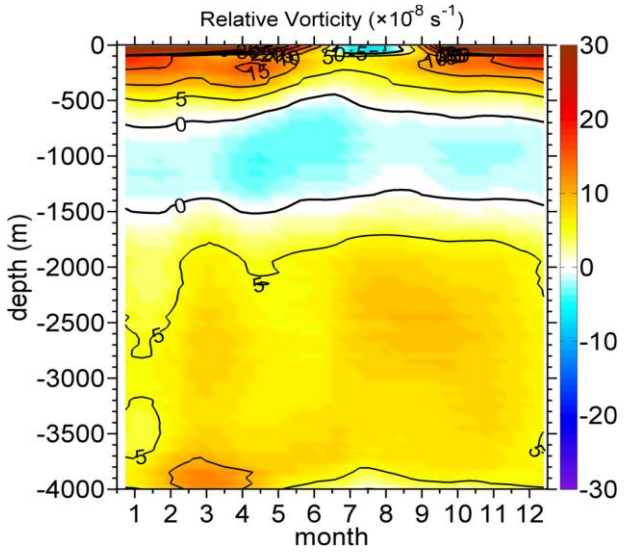

Fig. 4. Time series of domain-averaged depth-dependent relative vorticity in the SCS basin (>100 m) (adapted from Gan et al. 2016b).

3.2 Characteristics of thermohalines

Fig. 5a displays the horizontal distribution of the density anomaly, $\rho_\theta{}'$, at representative layers of the World Ocean Atlas 2013 (WOA13). We use this horizontal distribution to identify hydrographic properties of SCS water.

At different locations (x, y, z) in the SCS, $\rho_\theta{}'$ is expressed as

$$\rho_\theta{}'(x,y,z) = \rho_\theta(x,y,z) - \overline{\rho_\theta}(z), \tag{2}$$

where $\overline{\rho_\theta}(z) = \frac{\iint_{SCS}\rho_\theta(x,y,z)dxdy}{\iint_{SCS}dxdy}$ represents the horizontally averaged $\overline{\rho_\theta}$.

Fig. 5b illustrates the zonally averaged $\rho_\theta{}'$ in the basin.

In Fig. 5a, we see that upwelling of denser intermediate water occurs in the northern and western SCS, immediately beneath the mixed layer (200 m and 500 m), where there is positive $\rho_\theta{}'$. It is possible for the lighter water in the upper layer to be subducted into the intermediate layer

in the SSCS where ρ_θ' is negative at 200 m and 500 m. However, the figure shows that there is extensive subduction of the upper layer water into the intermediate layer at 1000 m (negative ρ_θ'), and notable upwelling (positive ρ_θ') in the lower layer in the SSCS. More vertical migrations of water masses in the SSCS are indicated by the respective negative and positive ρ_θ' in the intermediate and lower (>1500 m) layers in Fig. 5b. Similarly, extensive downwelling of intermediate water towards the lower layer occurs in the NSCS, where ρ_θ' is negative (Fig. 5a).

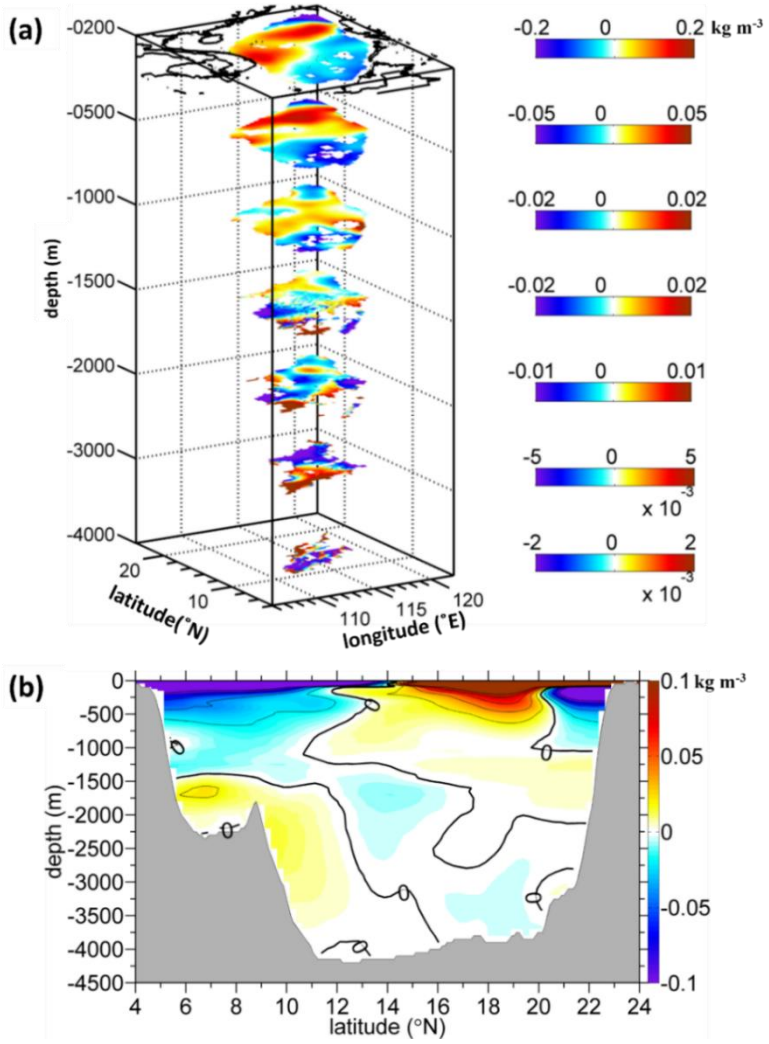

Fig. 5. (a) Three-dimensional view of ρ_θ' at selected, but representative, layers of the SCS and (b) zonally averaged ρ_θ' (kg m^{-3}) as a function of depth and latitude in the SCS. ρ_θ' is retrieved from the annual means of the WOA13 dataset (adapted from Liu and Gan 2017).

3.3 Circulation pathways and residence time

Studying the circulation pathways and knowing the residence time of the different water masses inform us about physical mechanisms driving the circulation in semi-enclosed systems. The residence times (ReT) of the different SCS waters have complicated spatial variability because the circulation is driven by internal and external forces and the circulation and thermal dynamics within the basin itself. Liu and Gan (2017) investigated the spatial variability of the residence time with a numerical Eulerian analysis on the Lagrangian characteristics of the SCS water masses. Fig. 6 is from Liu and Gan (2017) and illustrates the time series of the percentage of SCS water being replaced by the invasive non-SCS water as a function of the water depth. In Fig. 6, the 100% contour (bold black line) represents the time when the basin is completely occupied by non-SCS waters at certain depths and is called the maximum ReT (ReT_{max}). The relationship between the ReT and ReT_{max} is

$$ReT_{max}\,(\mathrm{z}) = \max[ReT(x, y, z)] \quad (3)$$

ReT_{max} for the entire SCS is generally shorter than 45 years. Fig. 6 illustrates that ReT_{max} increases with depth. It takes about three years for the water in the near-surface layer (< 200 m) to refresh. These SCS waters are replaced by the Kuroshio water cyclonically spreading over the upper layer.

ReT_{max} in the upper layer, where the pycnocline is located, rapidly increases to approximately 32 years at 750 m. ReT_{max} keeps increasing to its maximum in the intermediate layer (~42 years) and the upper part of the lower (~44 years) layer. In the closed less stratified basin, ReT_{max} reduces to approximately 40 years.

There is a narrow but deep trough (~2430 m) between 114-117°E and 6-8°N in the southernmost of the intermediate SSCS water. The water in the trough has limited communication with the rest of the SCS waters. This limitation causes a sharp increase of ReT_{max} at ~2200 m.

The amount of time needed to replace 90% of the SCS water masses in the water column further confirms that the longest ReT_{max} mainly occurs in the intermediate layer, because it takes ~38 years for 90% of the intermediate water to be refreshed, while it takes ~33 years to refresh the water in the lower layer. Unlike results from previous studies (for example, Yang et al. (2012)), the ReT_{max} increases monotonically with depth, and the maximum ReT_{max} in the intermediate

layer suggests that the formation of intermediate water is deferred if the prevailing circulation is anticyclonic.

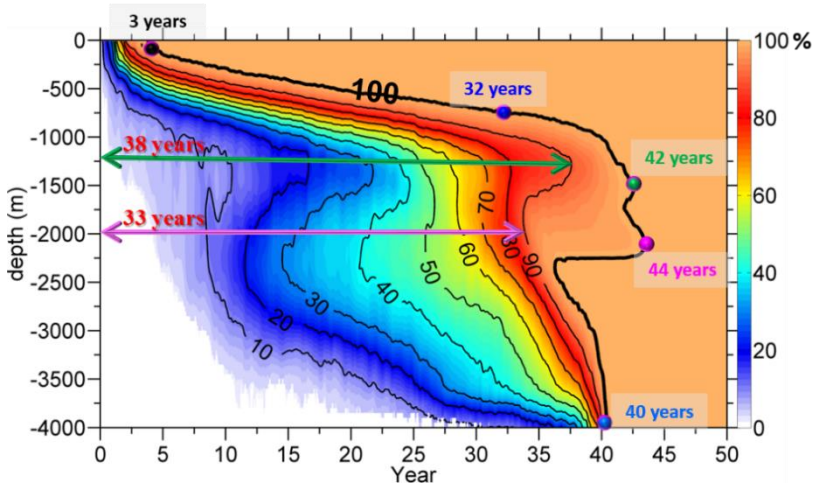

Fig. 6. Time series of the percentage of water that is refreshed in the SCS as a function of depth (adapted from Liu and Gan 2017).

4. The changing SCS circulation

Having described the fundamental characteristics and physics of the SCS circulation, we now discuss bi-decadal changes in the SCS circulation from 1992 to 2011.

4.1 Changes in horizontal plane

To discuss the recent changes in the circulation of the SCS, we use the surface velocity vectors averaged over 20 years from 1992 to 2011and the standard deviation from the mean velocity for that period. We present the surface vectors and standard deviations in Fig. 7. The figure illustrates the major characteristics and variability in the SCS circulation that link the westward intrusion of the Kuroshio through LS with the pathways of the SCSTF.

The mean circulation pattern is like the pattern we presented in the previous sections with a relatively large variance of the surface flow occurring near the entrance of LS and in the southwestern basin. Furthermore, the magnitudes of the variances in these two locations were comparable with their mean values, but the influences on the variability in the two locations are different.

The variability of the circulation near LS is associated with the variations of intensity and the path of Kuroshio intrusion at inter-annual, seasonal, and smaller temporal scales (Gan et al.

2016b). In the southwestern basin, the variability is associated with an opposing seasonal variation that is governed by a separating along-slope current off Vietnam associated with the southward slope current in winter and with the local wind stress curl dipole in summer (Gan et al. 2008). The strong southwestward slope current has a weak standard deviation in the northwestern slope that suggests that the current on the northwestern slope prevails all year.

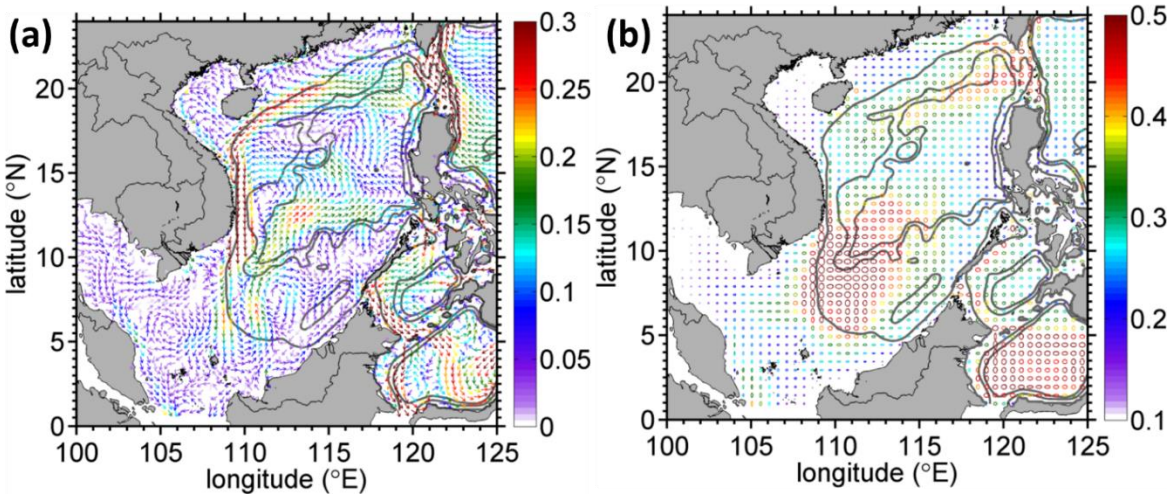

Fig. 7. (a) Long-term (1992 to 2011) averaged surface velocity vectors (m s^{-1}) and (b) associated standard deviation of the velocity vector in the SCS. The black contours are the 200, 2000, and 3000 m isobaths. The size and color of the circles in (b) indicate the magnitude of the standard derivation.

Seasonal cyclonic circulation in the upper layer is attributed to the positive vorticity in the slope current along the SCSTF. Like the surface velocity fields in Fig. 7, the larger variance of the cyclonic circulation occurs along the basin-wide slope current (Fig. 8). Variabilities from the Kuroshio intrusion and wind stress curl are the major drivers for the cyclonic circulation variabilities in the upper layer. In addition, spatial variation of the vorticity variance suggests that the local dynamics, such as the seasonally reversed jet along the steep slope off Vietnam (Gan and Qu 2008), contribute substantially to the upper layer circulation variability in the SCS. The circulation in the middle and deep layers (not shown) varies similarly to the upper layer.

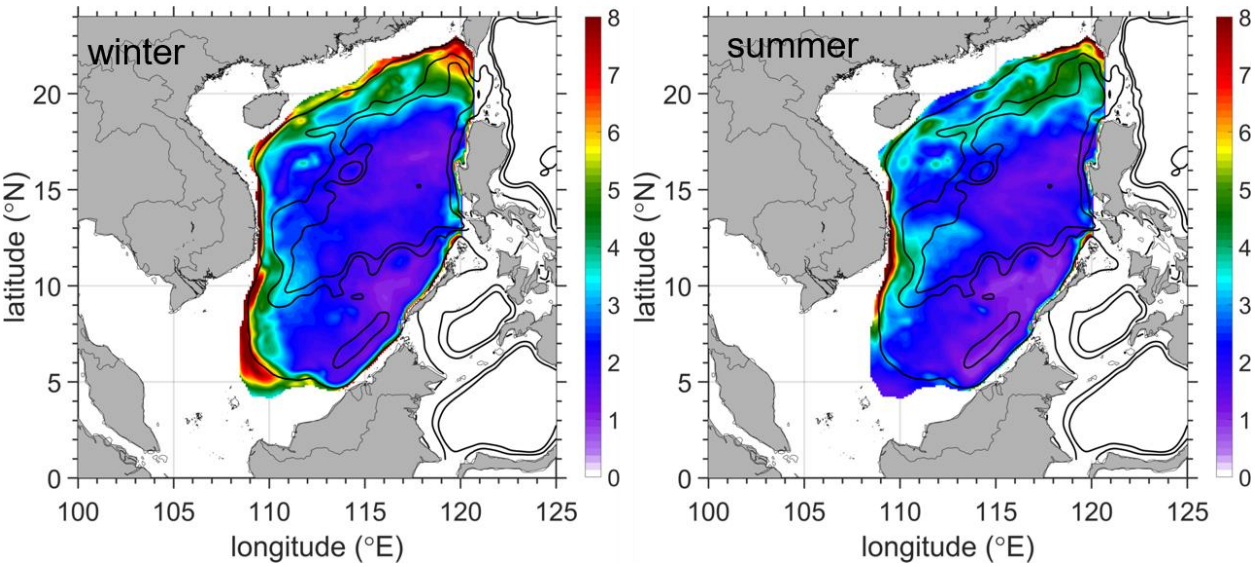

Fig. 8. Seasonal standard deviation of relative vorticity (10^{-6} s^{-1}) in the upper layer during the winter and summer from 1992 to 2011. The black contours are the 200, 2000, and 3000 m isobaths.

4.2 SCS layered circulation trends

As we have already discussed, the CAC circulation in the SCS has strong seasonal variability related to the Kuroshio intrusion and wind stress curl seasonality. However, the variability in the circulation also occurs in different frequency bands that are subject to the external controls of the Kuroshio intrusion and wind stress curl.

Fig. 9 shows the time series of the CAC circulation anomaly in the water column from 1992 to 2011 that we derived from the daily-averaged velocities from CMOMS output. While the CAC circulation prevails during these 20 years, the circulation exhibits a strong temporal variability at different frequencies. For the upper layer, the associated power spectrum density (not shown) indicates that the basin-averaged vorticity in that layer has significant periods of variation at six months, annual, and five-year cycles, which might be related to the annual and inter-annual variations of the circulation. Similar conditions exist in the middle and deep layers with the addition of a significant period at 2.5-years.

The cyclonic layers in the CAC circulation intensify over the 20 years (Fig. 9) while the anticyclonic circulation in the middle layer weakens. The increasing rates of vorticity for the cyclonic circulation in the upper (2.95×10^{-12} s^{-1} day^{-1}) and deep (2.35×10^{-12} s^{-1} day^{-1}) layers have similar magnitudes. However, the weakening rate of the anticyclonic circulation in the middle

(7.19×10^{-13} s^{-1} day^{-1}) layer is one order of magnitude smaller than the rates in the other layers. Despite the difference, the rate in the middle layer is still significant for those 20 years. The intensities of the domain- and time-averaged vorticities are stronger in the upper (1.45×10^{-7} s^{-1}) and deep (1.29×10^{-7} s^{-1}) layers, than in the middle (-1.04×10^{-9} s^{-1}) layer.

Gan et al. (2019) validated the trends in vorticity described in the previous paragraph using geostrophic currents derived from hydrographic data from the World Ocean Database (Boyer et al. 2018) and from the Archiving, Validation, and Interpretation of Satellite Oceanographic Data (AVISO; https://www.aviso.altimetry.fr/en/home.html) dataset. The changing CAC circulation has rarely been studied, and the cause of the changes is largely unclear. Nevertheless, there is the belief that the circulation changes are controlled by corresponding changes in the wind stress curl and the net planetary vorticity influx from the SCS's surrounding straits (Gan et al. 2016a).

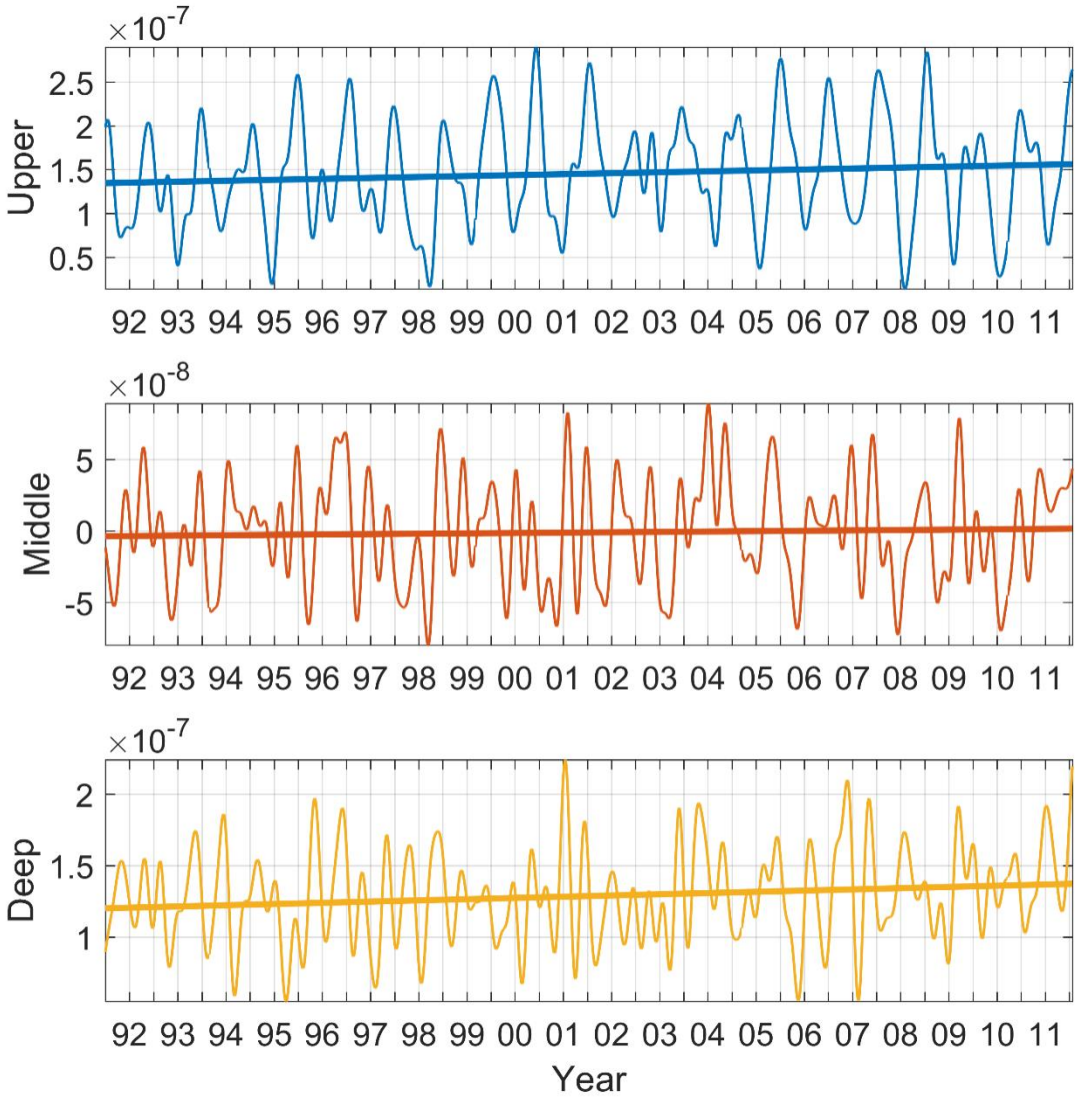

Fig. 9. Time series of 90-day filtered, layer-integrated, and basin-averaged vorticity (s^{-1}) from the upper, middle, and deep layers. The straight lines are the corresponding trends with rates of k_1=2.95×10^{-12}, k_2=7.19×10^{-13}, and k_3=2.35×10^{-12} s^{-1} day^{-1} from 1992 to 2011. All trend rates (k) pass 95% significance. Areas with water depth shallower than 100 m in the basin are excluded in the calculation.

5. Dynamics for the changing SCS circulation

5.1 Vorticity dynamics

In this section, we describe the fundamental forcing mechanism for the SCS circulation using vorticity dynamics (Gan et al. 2016a).

With Stokes' theorem, the circulation is expressed as the sum of the vertical relative vorticity over that region (Equation 4). Integrating the Layer-Integrated Vorticity Equation (LIVE) (Gan et al. 2016a) over the entire domain identifies the multi-forcing mechanisms of wind, lateral fluxes, and the intrinsic dynamics of the flow-topography interaction, and identifies their contribution to the circulation.

LIVE is written as:

$$\overbrace{\int_A \Omega_t \, dA}^{\Omega^{\mathrm{acce}}} = \overbrace{-\int_A [(f\bar{u}D)_x + (f\bar{v}D)_y] \, dA}^{\Omega^{cor}} \overbrace{-\int_A \nabla_H \times (\mathbf{HNL}) \, dA + \int_A \nabla \times \int_{Lb}^{Lu} \mathbf{hvisc} \, dz \, dA}^{\Omega^{hadv}} \overbrace{-\int_A \nabla_H \times (\mathbf{VNL}) \, dA}^{\Omega^{vadv}} + \overbrace{\int_A -\frac{1}{\rho_o}[J(LB, P^{Lb}) + J(Lu, P^{Lu})] dA}^{\Omega^{pgf}} + \overbrace{\int_A \nabla_H \times \int_{Lb}^{Lu} (K_v(\bar{\mathbf{v}})_z)_z \, dz dA}^{\Omega^{vvis}} ; \quad (4)$$

for the upper layer, $Lu = \eta$ and $Lb = \begin{cases} h(x,y), -750 < h < -100 \, m \\ -750 \, m, \quad h \geq -750 \, m \end{cases}$;

for the middle layer, $Lu = -750 \, m$ and $Lb = \begin{cases} h(x,y), -1500 < h < -750m \\ -1500 \, m, \quad h \geq -1500 \, m \end{cases}$;

and for the bottom layer, $Lu = -1500$ and $Lb = h(x,y)$.

f is the Coriolis parameter. D is the total layer depth. u and v are the zonal (x) and meridional (y) velocities, respectively. Lu and Lb are the depths of the top and bottom for each specific layer, respectively. η is the sea surface elevation. **HNL** is the horizontal nonlinear advection. **hvisc** is the horizontal viscous term, which is generally very small. **VNL** is the vertical advection term. P^{Lu} and P^{Lb} are the pressure at the top and bottom of each specific layer, respectively. J is a Jacobian operator. K_v is the vertical viscous coefficient. The suffix represents derivation, and the overbar refers to the layer average.

The physical meaning of each term in LIVE, from left to right, is the acceleration Ω^{acce}, divergence Ω^{cor} (vortex stretching and β-effect), the horizontal advection Ω^{hadv}, tilting Ω^{vadv}, pressure torque Ω^{pgf}, and vertical viscosity Ω^{vvis}. Ω^{vvis} can be expressed as $\Omega^{vvis} = \Omega^{sstr}$ (wind stress curl) $-\Omega^{bstr}$ (bottom stress curl) in the upper layer. The bottom pressure torque, Ω^{pgf}, forms when the baroclinic induced pressure interacts with the variable slope topography (Mertz and Wright 1992). The nonuniform vertical velocity field generates tilting horizontal components of

the vorticity into the vertical and causes tilting Ω^{vadv}. Fig. 10 demonstrates how the terms in Equation (4) balance for each layer.

5.2 Dynamic driver for the CAC circulation

In this section, we discuss the balance of the LIVE terms using the model results from CMOMS forced with climatological mean atmospheric fluxes (Gan et al. 2016b).

The winter model results attribute the major sources of the SCS upper layer cyclonic circulation to Ω^{cor} and Ω^{sstr}. The two terms are mainly balanced by Ω^{pgf} and Ω^{bstr}. The main sources for the relatively weak cyclonic circulation in summer is Ω^{hadv} and Ω^{cor}. The Ω^{sstr} has a very small influence, and it is mainly balanced by Ω^{pgf}. The negative value of Ω^{acce}, in winter and summer, suggests that the cyclonic circulation weakens following accelerations in autumn and spring (Fig. 3).

In the middle and deep layers, the Ω^{cor} is the main source of the anticyclonic and cyclonic circulation. The bottom pressure torque Ω^{pgf} primarily balances Ω^{cor}, while the remaining terms are relatively small. Almost all the signs of the terms in the middle layer oppose those in the upper and deep layers.

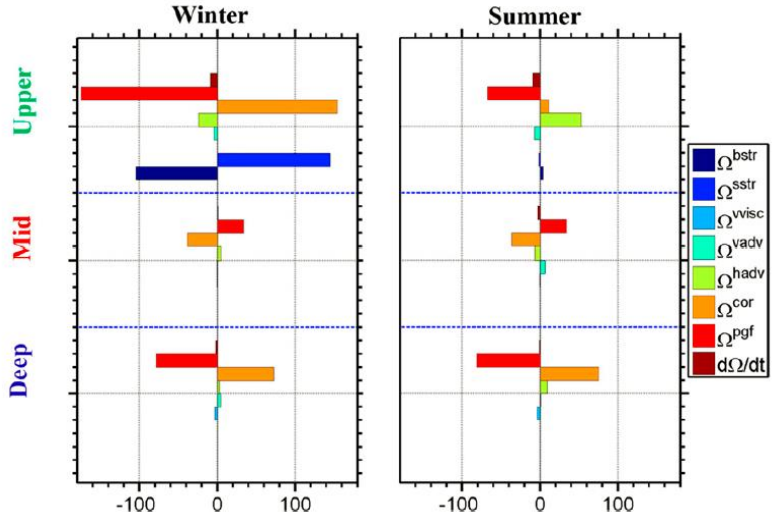

Fig. 10. Terms $(m^3 s^{-2})$ of the domain and layer integrated vorticity equation in the upper, middle (mid), and deep layers during (left) winter and (right) summer: Ω^{acce} is acceleration; Ω^{cor} is divergence or vortex stretching; Ω^{hadv} is horizontal advection; Ω^{vadv} is tilting; Ω^{pgf} is the bottom

pressure torque; Ω^{vvis} is vertical viscosity (middle and deep layers); Ω^{sstr} is wind stress curl; and Ω^{bstr} is bottom stress curl in the upper layer (adapted from Gan et al. 2016a).

Ω^{cor} is the dominant source of the CAC circulation in each layer, while Ω^{pgf} acts as the major response to CAC circulation in the SCS basin. According to the divergence theorem, the Ω^{cor} could be related to the planetary vorticity fluxes that cross the meridionally oriented section of LS. The same relationship could exist for the meridionally (*Si*) and zonally (*Sj*) oriented sections along Mindoro Strait and along the 100-m isobath. Equation 5 represents this relationship between Ω^{cor} and planetary vorticity fluxes. These planetary vorticity fluxes provide extrinsic vorticity sources for the CAC circulation in the SCS.

$$\Omega^{cor} = -\int_{Si} f\bar{u}\, dSi - \int_{Sj} f\bar{v}\, dSj. \quad (5)$$

Fig. 11 shows that the planetary vorticity flux through LS mainly contributes to Ω^{cor} in all the layers during winter and summer, while the planetary vorticity flux through Mindoro Strait and the 100-m isobath mainly offsets Ω^{cor}.

Therefore, we attribute the CAC circulation to vortex stretching from the planetary vortex that is extrinsically induced by the inflow-outflow-inflow in the upper-middle-deep layers through LS. Furthermore, we attribute the cyclonic circulation in the upper layer to wind stress curl in winter and nonlinear advection in summer (Gan et al. 2016a).

Overall, our results suggest that the changing CAC circulation in the SCS is largely controlled by the corresponding changes in planetary fluxes through the straits around the SCS and wind stress curl. However, the variability of the CAC circulation can also arise from the response of flow to the slope topography and from the nonlinearity of the circulation itself, as the relatively large magnitudes of bottom pressure torque Ω^{pgf} and horizontal advection Ω^{hadv} show.

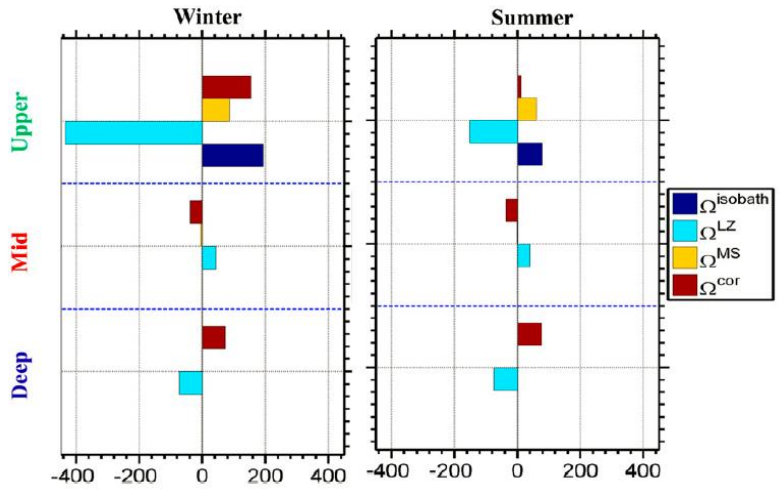

Fig. 11. Mean values of Ω^{cor} terms (m^3s^{-2}) in the upper, middle (mid), and deep layers and the respective contributions by planetary vorticity flux through Luzon Strait Ω^{LZ}, Mindoro Strait Ω^{MS}, and across the 100-m isobath $\Omega^{isobath}$ in winter and summer (adapted from Gan et al. 2016a).

5.3 Mechanism for the changing layered circulation

Equations 4 and 5 show us that external forcing of monsoonal wind stress curl and planetary vorticity flux from the external inflow/outflow through the straits around the SCS mainly drive the circulation in the SCS (also see Gan et al. 2016b). We also see that corresponding internal responses include bottom pressure torque arising from the flow interacting with the continental slope, a vertical exchange of vorticity among layers, and other nonlinear dynamic processes. We now discuss the mechanism that drives the changes in the CAC circulation occurring over our 20-year study period.

During our 20-year study period, the net planetary vorticity flux in the upper layer through all straits weakens (Gan et al. 2019). This weakening is due to the decreased Kuroshio intrusion into the basin from LS, because of an intensifying Kuroshio (Fig. 12). We found that the Kuroshio intrusion increased at the rate of k=7.11×10^{-5} Sv day^{-1} over the 20 years. Nan et al. (2016) observed that the upper layer freshened in the SCS from 1993 to 2012, which they attributed to the weakening of the Kuroshio intrusion through LS. The decreasing trend of the planetary vorticity influx would weaken the cyclonic circulation in the upper CAC circulation according to Equations 4 and 5, so decreasing planetary vorticity cannot account for the strengthened cyclonic circulation in the upper layer shown in Fig. 9.

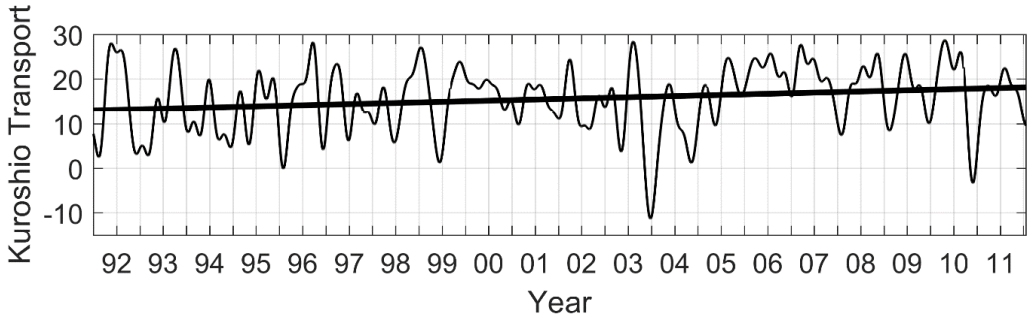

Fig. 12. Time series of Kuroshio transport (Sv) along 18°E from the coast to 130°E. The thick black line indicates the trend of the transport which has a rate of k=7.11×10^{-5} Sv day^{-1} with 95% significance.

Equation 3 shows that a change of wind stress curl can alter vorticity. Our data show that the basin-averaged wind stress curl is positive in all seasons (Gan et al. 2016b). During the 20-year period, the basin-integrated wind stress curl ($\nabla \times \tau^s \frac{\tau s}{\rho}$) strengthens at a rate of k=0.0044 m^{3}s^{-2} day^{-1} (with 95% significance). The increasing wind stress curl imparts positive vorticity to strengthen the upper cyclonic circulation and modulates the dynamic height at the surface which could affect the overall changing circulation in the water column through a spin-up/spin-down of the barotropic pressure gradient.

The strengthening cyclonic circulation in the deep layer of the semi-closed basin (Fig. 9) is due to the increase in deep planetary vorticity influx through LS (Table 1, Gan et al. 2019). The reason for the increasing deep intrusion through LS is unknown.

The strengthening middle layer outflow through LS represents a loss of planetary vorticity for the layer so it cannot account for the weakening anticyclonic circulation in the middle layer. The viscous drag curl (Ω^{vvis} in Equation 4) from the increasing cyclonic circulation in the neighboring upper and deep layers would contribute to the decelerating anticyclonic in the middle layer. In addition, the vertical vorticity flux from the neighboring layers could contribute to the weakening anticyclonic circulation in the middle layer.

The changing external forcing for the CAC circulation has been related to the Pacific Decadal Oscillation (PDO) in previous studies (Nan et al. 2016), but more analyses are required before we can provide a holistic understanding of the mechanism that changes the CAC circulation,

in particular the change in the middle and deep layers. We still lack understanding of the deep circulation pattern in the tropical NPO off LS.

Table 1 summarizes the trends of the CAC circulation, the corresponding planetary vorticity flux through LS, and the domain-averaged wind stress curl. Gan et al. (2019) present the detailed mechanism governing the variability and long-term trend in the CAC circulation in the SCS.

Variables / Layer	Vorticity	F flux into basin	WSC
Upper	+	-	+
Middle	+	-	
Deep	+	+	

Table 1. Trends of basin-averaged vorticity, net planetary vorticity flux (F flux) into the basin, and wind stress curl. The symbol "+" indicates an increasing rate and "-" denotes a decreasing trend.

6. Summary

In this chapter, we outline the characteristics of the SCS circulation based on recent research derived from observations and numerical simulations. We present the three-layer alternating CAC circulation in the SCS based on Stokes' Theorem. We dynamically link the CAC circulation with the extrinsic forcing of winds and lateral momentum/vorticity fluxes through the straits around the SCS. We also bridge the extrinsic forcing and intrinsic dynamic response in the CAC circulation in the SCS basin. We use the CAC circulation to derive the pathways and residence time of the water masses in the SCS.

Our new fundamental knowledge about the SCS circulation shows us the long-term trends and variability of the CAC circulation. The changing circulation provides a broad dynamic overview of the response of a regional ocean such as SCS to changing forcing in the large-scale tropical NPO and atmospheric fluxes. These findings provide new understanding of the changing circulation patterns, hydrographic properties, energy, and biogeochemical substances in the SCS.

The three-dimensional SCS circulation characterized by the vertically alternating spinning CAC circulation in the upper, middle, and deep layers, is mainly driven by the net planetary

vorticity influx/outflux through the straits surrounding the SCS. We find that the CAC circulation is mainly composed of basin-wide slope currents. The vorticity of the CAC circulation comes primarily from the vorticities arising along the route of the SCSTF in the slope current, the Kuroshio intrusion near LS, and outflow near Mindoro Strait in the upper and middle layers. A larger contribution to the cyclonic circulation in the deep layer is from the circulation in the southwestern deep basin.

The CAC circulation displays strong spatiotemporal variability over a 20-year study period, from 1992 to 2011. The largest variances are mainly along the stream of the SCSTF over the slope, and there is a strengthening trend of the CAC circulation in the SCS. This changing circulation is caused by a corresponding strengthening positive wind stress curl in the upper layer. The mechanism that leads to the strengthening of the circulation in the middle and deep layers is not obvious and needs further investigation. The underlying driver(s) for the changing CAC circulation is complex and may be associated with the changing oceanic circulation in the tropical NPO, influx/outflux through the straits, and the changing vertical exchanges among the three layers.

Understanding the fundamental dynamics that regulate the CAC circulation is essential for identifying the process that leads to the changing CAC circulation. We use a dynamic tool, based on LIVE to bridge extrinsic and intrinsic forcing, to diagnose the underlying physics. This tool is critical in forecasting the trend of the changing SCS circulation. We find that the CAC circulation forms, because of the vorticity imparted by wind stress curl of the East Asia monsoon and, the input of planetary vorticity flux from the inflow-outflow-inflow in LS after the input has been offset by the vorticity induced by the interacting baroclinic flow and basin topography or bottom pressure torque.

We find that the inflow-outflow-inflow in LS persisted for our 20-year study from 1992-2011, and the variability occupies different frequency bands. The variation of the inflow/outflow in LS is related to the intensity of the Kuroshio in the upper layer, which, in turn, is linked with the NPO currents: the NEC, Kuroshio, and Mindanao Current. Similarly, the CAC circulation in the middle and deep layers link to the corresponding under currents of the North Equatorial Undercurrent, Luzon Undercurrent, and Mindanao Undercurrent. The results derived from LIVE show that the changing extrinsic fluxes would alter the total budget of the planetary vorticity and

trigger corresponding intrinsic dynamics of the interacting flow topography and associated nonlinear processes in the CAC circulation.

In the end, though, we still have little knowledge about how the responses of the intrinsic dynamics interact with the extrinsic forcing to regulate the changing SCS circulation. We lack understanding about the variability of the current system in the NPO, particularly regarding the role of undercurrents on the CAC circulation. Understanding the interaction between the forcing and resulting flow and the variable NPO currents are essential for us to completely understand the changing ocean circulation, the regional climate variability, transport of biogeochemical substances in the SCS and overall understanding of ocean science development in this marginal sea.

Acknowledgements. This research was supported by the National (China) Key Basic Research Development Program (2015CB954004), and the Hong Kong Research Grants Council (GRF16204915, GRF16206516).

References

Boyer T P, Baranova O K, Coleman C et al (2018) World Ocean Database 2018 In: Mishonov A V Technical Editor, NOAA Atlas NESDIS 87,

Cai Z Y, Gan J P, Liu Z Q et al (2019) Progress on the formation dynamics for the layered circulation in the South China Sea. Prog. in Oceangr (submitting)

Chao S Y, Shaw P T, and Wu S Y (1996) Deep water ventilation in the South China Sea. Deep-Sea Res Pt I 43(4):445-466, doi:Doi 10.1016/0967-0637(96)00025-8

Fang G, Wang Y, Wei Z et al(2009) Interocean circulation and heat and freshwater budgets of the South China Sea based on a numerical model. Dynamics of Atmospheres and Oceans 47(1): 55-72.

Gan J P and Qu T (2008) Coastal jet separation and associated flow variability in the southwest South China Sea Deep-Sea Res Pt I 55(1):1-19. doi:DOI 10.1016/j.dsr.2007.09.008.

Gan J P, Cheung A, Guo X G et al (2009a) Intensified upwelling over a widened shelf in the northeastern South China Sea. J. Geophys. Res.-Oceans 114(C9)

Gan J P, Li H, Curchitser E N et al(2006) Modeling South China Sea circulation: Response to seasonal forcing regimes. J. Geophys. Res.-Oceans 111(C6)

Gan J P, Li L, Wang D X et al(2009b) Interaction of a river plume with coastal upwelling in the northeastern South China Sea. Continental Shelf Res. 29(4):728-740

Gan J P, Liu Z Q, and Hui C R (2016a) A three-layer alternating spinning circulation in the South China Sea. J. Phys. Oceanogr. 46(8): 2309-2315

Gan J P, Liu Z Q , and Liang L L (2016b) Numerical modeling of intrinsically and extrinsically forced seasonal circulation in the China Seas: a kinematic study. J. Geophys. Res.-Oceans, 121(7):4697-4715

Gan J P, Cai Z, Tang Y et al(2019) Chaniging layered circulation in the South China Sea and adjacent northwestern Pacific Ocean (1992-2011). (to be submitted to *Nat. Geosci.*)

Hellerman S and Rosenstein M (1983) Normal monthly wind stress over the world ocean with error-estimates. J. Phys. Oceanogr. 13(7): 1093-1104

Hsin Y C,Wu C R and Chao S Y (2012) An updated examination of the Luzon Strait transport. J. Geophys. Res.-Oceans 117,C03022.

Lan J, Zhang N N, and Wang Y (2013) On the dynamics of the South China Sea deep circulation. J. Geophys. Res.-Oceans 118(3): 1206-1210

Li L and Qu T D(2006) Thermohaline circulation in the deep South China Sea basin inferred from oxygen distributions. J. Geophys. Res.-Oceans 111(C5)

Liu Z and Gan J (2017) Three-dimensional pathways of water masses in the South China Sea: a modeling study. J. Geophys. Res.-Oceans 122(7): 6039-6054

Liu Z Q and Gan J P(2012) Variability of the Kuroshio in the East China Sea derived from satellite altimetry data. Deep-Sea Res. Pt. I 59: 25-36, doi:10.1016/j.dsr.2011.10.008.

Mertz G and Wright D G (1992) Interpretations of the JEBAR term. J. Phys. Oceanogr. 22(3): 301-305

Nan F, Xue H J, and Yu F (2015) Kuroshio intrusion into the South China Sea: A review. Prog. in Oceangr. 137:314-333

Nan F, Yu F, Xue H, Zengb L et al (2016) Freshening of the upper ocean in the South China Sea since the early 1990s. Deep-Sea Res. I 118:20-29

Qu T (2000) Upper-layer circulation in the South China Sea. J. Phys. Oceanogr. 30(6):1450-1460

Qu T,Mitsudera H, and Yamagata T(2000) Intrusion of the North Pacific waters into the South China Sea. J. Geophys. Res.-Oceans 105(C3):6415-6424

Qu T D, Du Y, and Sasaki H(2006) South China Sea throughflow: A heat and freshwater conveyor. Geophys. Res. Lett. 33(23)

Qu T D,Song Y T, andYamagata T (2009) An introduction to the South China Sea throughflow: Its dynamics, variability, and application for climate. Dynamics Of Atmospheres And Oceans 47(1-3):3-14.

Wang G H, Xie S P, Qu T D et al(2011) Deep South China Sea circulation. Geophys. Res. Lett. 38(5)

Wu C R, and Hsin Y C (2012) The forcing mechanism leading to the Kuroshio intrusion into the South China Sea. J. Geophys. Res.-Oceans (1978–2012) 117(C7)

Xu F H and Oey L Y (2014) State analysis using the Local Ensemble Transform Kalman Filter (LETKF) and the three-layer circulation structure of the Luzon Strait and the South China Sea. Ocean Dynamics 64(6):905-923

Yang S C, Lee D C, and Ho T Y(2012) The isotopic composition of Cadmium in the water column of the South China Sea. Geochimica Et Cosmochimica Acta 98: 66-77